






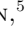




























Search for joint multimessenger signals from potential Galactic PeVatrons with HAWC and IceCube

R. ALFARO,¹ C. ALVAREZ,² J.C. ARTEAGA-VELÁZQUEZ,³ D. AVILA ROJAS,¹ H.A. AYALA SOLARES ,⁴ R. BABU,⁵
E. BELMONT-MORENO,¹ K.S. CABALLERO-MORA,² T. CAPISTRÁN ,⁶ A. CARRAMIÑANA,⁷ S. CASANOVA ,⁸ U. COTTI ,³
J. COTZOMI ,⁹ S. COUTIÑO DE LEÓN,¹⁰ E. DE LA FUENTE ,¹¹ D. DEPAOLI,¹² N. DI LALLA,¹³ R. DIAZ HERNANDEZ,⁷
J.C. DÍAZ-VÉLEZ ,¹⁰ K. ENGEL ,¹⁴ T. ERGIN,⁵ K.L. FAN ,¹⁴ K. FANG ,¹⁰ N. FRAIJA,⁶ S. FRAIJA,⁶
J.A. GARCÍA-GONZÁLEZ ,¹⁵ F. GARFIAS ,⁶ M.M. GONZÁLEZ ,⁶ J.A. GOODMAN ,¹⁴ S. GROETSCH,¹⁶ J.P. HARDING,¹⁷
S. HERNÁNDEZ-CADENA,¹⁸ I. HERZOG,⁵ D. HUANG ,¹⁴ F. HUEYOTL-ZAHUANTITLA ,² P. HÜNTEMEYER,¹⁶ A. IRIARTE ,⁶
S. KAUFMANN,¹⁹ J. LEE ,²⁰ H. LEÓN VARGAS ,^{1,7} G. LUIS-RAYA ,¹⁹ K. MALONE ,¹⁷ J. MARTÍNEZ-CASTRO,²¹
J.A. MATTHEWS ,²² P. MIRANDA-ROMAGNOLI,²³ J.A. MONTES,⁶ E. MORENO,⁹ M. MOSTAFÁ ,²⁴ L. NELLEN ,²⁵
M.U. NISA ,⁵ N. OMODEI ,¹³ M. OSORIO,⁶ Y. PÉREZ ARAUJO ,⁶ E.G. PÉREZ-PÉREZ ,¹⁹ C.D. RHO ,²⁶
D. ROSA-GONZÁLEZ ,⁷ H. SALAZAR,⁹ D. SALAZAR-GALLEGOS,⁵ A. SANDOVAL,¹ M. SCHNEIDER,¹⁴ J. SERNA-FRANCO,¹
A.J. SMITH,¹⁴ Y. SON,²⁰ O. TIBOLLA,¹⁹ K. TOLLEFSON ,⁵ I. TORRES ,⁷ R. TORRES-ESCOBEDO,¹⁸ R. TURNER,¹⁶
F. UREÑA-MENA,⁷ X. WANG,¹⁶ I.J. WATSON,²⁰ K. WHITAKER,⁴ E. WILLOX,¹⁴ H. WU,¹⁰ S. YU ,⁴ S. YUN-CÁRCAMO ,¹⁴
H. ZHOU,¹⁸ C. DE LEÓN,³

HAWC COLLABORATION

R. ABBASI ,²⁷ M. ACKERMANN ,²⁸ J. ADAMS,²⁹ S. K. AGARWALLA ,^{10,*} J. A. AGUILAR ,³⁰ M. AHLERS ,³¹
J.M. ALAMEDDINE ,³² N. M. AMIN,³³ K. ANDEEN ,³⁴ C. ARGÜELLES ,³⁵ Y. ASHIDA,³⁶ S. ATHANASIADOU,²⁸
L. AUSBORM,³⁷ S. N. AXANI ,³³ X. BAI ,³⁸ A. BALAGOPAL V. ,¹⁰ M. BARICEVIC,¹⁰ S. W. BARWICK ,³⁹ S. BASH,⁴⁰
V. BASU ,¹⁰ R. BAY,⁴¹ J. J. BEATTY ,^{42,43} J. BECKER TJUS ,^{44,†} J. BEISE ,⁴⁵ C. BELLENGHI ,⁴⁰ C. BENNING,³⁷
S. BENZVI ,⁴⁶ D. BERLEY,¹⁴ E. BERNARDINI ,⁴⁷ D. Z. BESSON,⁴⁸ E. BLAUFUSS ,¹⁴ L. BLOOM ,⁴⁹ S. BLOT ,²⁸
F. BONTEMPO,⁵⁰ J. Y. BOOK MOTZKIN ,³⁵ C. BOSCOLO MENEGUOLO ,⁴⁷ S. BÖSER ,⁵¹ O. BOTNER ,⁴⁵
J. BÖTTCHER ,³⁷ J. BRAUN,¹⁰ B. BRINSON ,⁵² J. BROSTEAN-KAISER,²⁸ L. BRUSA,³⁷ R. T. BURLEY,⁵³
D. BUTTERFIELD,¹⁰ M. A. CAMPANA ,⁵⁴ I. CARACAS,⁵¹ K. CARLONI,³⁵ J. CARPIO ,^{55,56} S. CHATTOPADHYAY,^{10,*}
N. CHAU,³⁰ Z. CHEN,⁵⁷ D. CHIRKIN ,¹⁰ S. CHOI,^{58,59} B. A. CLARK ,¹⁴ A. COLEMAN ,⁴⁵ G. H. COLLIN,⁶⁰
A. CONNOLLY,^{42,43} J. M. CONRAD ,⁶⁰ P. COPPIN ,⁶¹ R. CORLEY,³⁶ P. CORREA ,⁶¹ D. F. COWEN ,^{62,4} P. DAVE ,⁵²
C. DE CLERCQ ,⁶¹ J. J. DELAUNAY ,⁴⁹ D. DELGADO ,³⁵ S. DENG,³⁷ A. DESAI ,¹⁰ P. DESIATI ,¹⁰
K. D. DE VRIES ,⁶¹ G. DE WASSEIGE ,⁶³ T. DEYOUNG ,⁵ A. DIAZ ,⁶⁰ J. C. DÍAZ-VÉLEZ ,¹⁰ P. DIERICHS,³⁷
M. DITTMER,⁶⁴ A. DOMI,⁶⁵ L. DRAPER,³⁶ H. DUJMOVIC ,¹⁰ K. DUTTA,⁵¹ M. A. DUVERNOIS ,¹⁰ T. EHRHARDT,⁵¹
L. EIDENSCHINK,⁴⁰ A. EIMER,⁶⁵ P. ELLER ,⁴⁰ E. ELLINGER,⁶⁶ S. EL MENTAWI,³⁷ D. ELSÄSSER ,³² R. ENGEL,^{50,67}
H. ERPENBECK ,¹⁰ J. EVANS,¹⁴ P. A. EVENSON,³³ K. FARRAG,⁶⁸ A. R. FAZELY ,⁶⁹ A. FEDYNITCH ,⁷⁰ N. FEIGL,⁷¹
S. FIEDLSCHUSTER,⁶⁵ C. FINLEY ,⁷² L. FISCHER ,²⁸ D. FOX ,⁶² A. FRANCKOWIAK ,⁴⁴ S. FUKAMI,²⁸ P. FÜRST ,³⁷
J. GALLAGHER,⁷³ E. GANSTER ,³⁷ A. GARCIA ,³⁵ M. GARCIA,³³ G. GARG,^{10,*} E. GENTON,^{35,63} L. GERHARDT,⁷⁴
A. GHADIMI ,⁴⁹ C. GIRARD-CARILLO,⁵¹ C. GLASER,⁴⁵ T. GLÜSENKAMP ,^{65,45} J. G. GONZALEZ,³³ S. GOSWAMI,^{55,56}
A. GRANADOS,⁵ D. GRANT,⁵ S. J. GRAY ,¹⁴ O. GRIES,³⁷ S. GRIFFIN ,¹⁰ S. GRISWOLD ,⁴⁶ K. M. GROTH ,³¹
C. GÜNTHER,³⁷ P. GUTJAHN ,³² C. HA,⁷⁵ C. HAACK ,⁶⁵ A. HALLGREN ,⁴⁵ L. HALVE ,³⁷ F. HALZEN ,¹⁰
H. HAMDAR ,⁵⁷ M. HA MINH,⁴⁰ M. HANDT,³⁷ K. HANSON,¹⁰ J. HARDIN,⁶⁰ A. A. HARNISCH,⁵ P. HATCH,⁷⁶
A. HAUNGS ,⁵⁰ J. HÄUSSLER,³⁷ K. HELBING ,⁶⁶ J. HELLRUNG ,⁴⁴ J. HERMANNSGABNER,³⁷ L. HEUERMAN,³⁷
N. HEYER ,⁴⁵ S. HICKFORD,⁶⁶ A. HIDVEGI,⁷² C. HILL ,⁶⁸ G. C. HILL,⁵³ K. D. HOFFMAN,¹⁴ S. HORI ,¹⁰
K. HOSHINA,^{10,‡} M. HOSTERT ,³⁵ W. HOU ,⁵⁰ T. HUBER ,⁵⁰ K. HULTQVIST ,⁷² M. HÜNNEFELD ,³² R. HUSSAIN,¹⁰
K. HYMON,³² A. ISHIHARA,⁶⁸ W. IWAKIRI ,⁶⁸ M. JACQUART,¹⁰ O. JANIK,⁶⁵ M. JANSSON,⁷² G. S. JAPARIDZE ,⁷⁷
M. JEONG ,³⁶ M. JIN ,³⁵ B. J. P. JONES ,⁷⁸ N. KAMP,³⁵ D. KANG ,⁵⁰ W. KANG ,⁵⁸ X. KANG,⁵⁴ A. KAPPES ,⁶⁴
D. KAPPESSER,⁵¹ L. KARDUM,³² T. KARG ,²⁸ M. KARL ,⁴⁰ A. KARLE ,¹⁰ A. KATIL,⁷⁹ U. KATZ ,⁶⁵ M. KAUER ,¹⁰
J. L. KELLEY ,¹⁰ M. KHANAL,³⁶ A. KHATEE ZATHUL ,¹⁰ A. KHEIRANDISH ,^{55,56} J. KIRYLUK ,⁵⁷ S. R. KLEIN ,^{41,74}
A. KOCHOCKI ,⁵ R. KOIRALA ,³³ H. KOLANOSKI ,⁷¹ T. KONTRIMAS ,⁴⁰ L. KÖPKE,⁵¹ C. KOPPER ,⁶⁵

Corresponding author: Kwok Lung Fan
klfan@umd.edu

Corresponding author: IceCube Collaboration
analysis@icecube.wisc.edu

D. J. KOSKINEN ³¹ P. KOUNDAL ³³ M. KOVACEVICH ⁵⁴ M. KOWALSKI ^{71,28} T. KOZYNETS,³¹
 J. KRISHNAMOORTHY ¹⁰, * K. KRUISWIJK ⁶³ E. KRUPCZAK,⁵ A. KUMAR ²⁸ E. KUN,⁴⁴ N. KURAHASHI ⁵⁴
 N. LAD ²⁸ C. LAGUNAS GUALDA ²⁸ M. LAMOUREUX ⁶³ M. J. LARSON ¹⁴ S. LATSEVA,³⁷ F. LAUBER ⁶⁶
 J. P. LAZAR ⁶³ J. W. LEE ⁵⁸ K. LEONARD DEHOLTEN ⁴ A. LESZCZYŃSKA ³³ J. LIAO ⁵² M. LINCETTO ⁴⁴
 Y. T. LIU,⁴ M. LIUBARSKA,⁷⁹ E. LOHFINK,⁵¹ C. LOVE,⁵⁴ C. J. LOZANO MARISCAL,⁶⁴ L. LU ¹⁰ F. LUCARELLI ⁸⁰
 W. LUSZCZAK ^{42,43} Y. LYU ^{41,74} J. MADSEN ¹⁰ E. MAGNUS ⁶¹ K. B. M. MAHN,⁵ Y. MAKINO,¹⁰ E. MANAO ⁴⁰
 S. MANCINA ^{10,47} W. MARIE SAINTE,¹⁰ I. C. MARIŞ ³⁰ S. MARKA ⁸¹ Z. MARKA ⁸¹ M. MARSEE,⁴⁹
 I. MARTINEZ-SOLER,³⁵ R. MARUYAMA ⁸² F. MAYHEW ⁵ F. MCNALLY ⁸³ J. V. MEAD,³¹ K. MEAGHER ¹⁰
 S. MECBAL,²⁸ A. MEDINA,⁴³ M. MEIER ⁶⁸ Y. MERCKX,⁶¹ L. MERTEN ⁴⁴ J. MICALLEF,⁵ J. MITCHELL,⁶⁹
 T. MONTARULI ⁸⁰ R. W. MOORE ⁷⁹ Y. MORI,⁶⁸ R. MORSE,¹⁰ M. MOULAI ¹⁰ T. MUKHERJEE ⁵⁰ R. NAAB ²⁸
 R. NAGAI ⁶⁸ M. NAKOS,¹⁰ U. NAUMANN,⁶⁶ J. NECKER ²⁸ A. NEGI,⁷⁸ L. NESTE ⁷² M. NEUMANN,⁶⁴
 H. NIEDERHAUSEN ⁵ K. NODA ⁶⁸ A. NOELL,³⁷ A. NOVIKOV,³³ A. OBERTACKE POLLMANN ⁶⁸ V. O'DELL ¹⁰
 B. OEYEN ⁸⁴ A. OLIVAS,¹⁴ R. ORSOE,⁴⁰ J. OSBORN,¹⁰ E. O'SULLIVAN ⁴⁵ H. PANDYA ³³ N. PARK ⁷⁶
 G. K. PARKER,⁷⁸ E. N. PAUDEL ³³ L. PAUL ³⁸ C. PÉREZ DE LOS HEROS ⁴⁵ T. PERNICE,²⁸ J. PETERSON,¹⁰
 S. PHILIPPEN ³⁷ A. PIZZUTO ¹⁰ M. PLUM ³⁸ A. PONTÉN,⁴⁵ Y. POPOVYCH,⁵¹ M. PRADO RODRIGUEZ,¹⁰ B. PRIES ⁵
 R. PROCTER-MURPHY,¹⁴ G. T. PRZYBYLSKI,⁷⁴ C. RAAB ⁶³ J. RACK-HELLEIS,⁵¹ M. RAVN,⁴⁵ K. RAWLINS,⁸⁵ Z. RECHAV,¹⁰
 A. REHMAN ³³ P. REICHERZER,⁴⁴ E. RESCONI ⁴⁰ S. REUSCH,²⁸ W. RHODE ³² B. RIEDEL ¹⁰ A. RIFAIE,³⁷
 E. J. ROBERTS,⁵³ S. ROBERTSON,^{41,74} S. RODAN,^{58,59} G. ROELLINGHOFF,⁵⁸ M. RONGEN ⁶⁵ A. ROSTED ⁶⁸
 C. ROTT ^{36,58} T. RUHE ³² L. RUOHAN,⁴⁰ D. RYCKBOSCH,⁸⁴ I. SAFA ¹⁰ J. SAFFER,⁶⁷ P. SAMPATHKUMAR,⁵⁰
 A. SANDROCK ⁶⁶ M. SANTANDER ⁴⁹ S. SARKAR ⁷⁹ S. SARKAR ⁸⁶ J. SAVELBERG,³⁷ P. SAVINA,¹⁰ P. SCHAILE,⁴⁰
 M. SCHAUFEL,³⁷ H. SCHIELER ⁵⁰ S. SCHINDLER ⁶⁵ B. SCHLÜTER,⁶⁴ F. SCHLÜTER ³⁰ N. SCHMEISSER,⁶⁶ T. SCHMIDT,¹⁴
 J. SCHNEIDER ⁶⁵ F. G. SCHRÖDER ^{50,33} L. SCHUMACHER ⁶⁵ S. SCLAFANI ¹⁴ D. SECKEL,³³ M. SEIKH ⁴⁸
 M. SEO,⁵⁸ S. SEUNARINE ⁸⁷ P. SEVLE MYHR ⁶³ R. SHAH,⁵⁴ S. SHEFALI,⁶⁷ N. SHIMIZU ⁶⁸ M. SILVA ¹⁰
 B. SKRZYPEK ⁴¹ B. SMITHERS ⁷⁸ R. SNIHUR,¹⁰ J. SOEDINGREKSO,³² A. SØGAARD,³¹ D. SOLDIN ³⁶ P. SOLDIN ³⁷
 G. SOMMANI ⁴⁴ C. SPANNFELLNER,⁴⁰ G. M. SPICZAK ⁸⁷ C. SPIERING ²⁸ M. STAMATIKOS,⁴³ T. STANEV,³³
 T. STEZELBERGER ⁷⁴ T. STÜRWARD,⁶⁶ T. STUTTARD ³¹ G. W. SULLIVAN ¹⁴ I. TABOADA ⁵²
 S. TER-ANTONYAN ⁶⁹ A. TERLIUK,⁴⁰ M. THIESMEYER,³⁷ W. G. THOMPSON ³⁵ J. THWAITES ¹⁰ S. TILAV,³³
 C. TÖNNIS,⁵⁸ S. TOSCANO ³⁰ D. TOSI,¹⁰ A. TRETTIN,²⁸ R. TURCOTTE,⁵⁰ J. P. TWAGIRAYEZU,⁵
 M. A. UNLAND ELORRIETA ⁶⁴ A. K. UPADHYAY ¹⁰, * K. UPSHAW,⁶⁹ A. VAIDYANATHAN,³⁴ N. VALTONEN-MATTILA ⁴⁵
 J. VANDENBROUCKE ¹⁰ N. VAN EIJNDHOVEN ⁶¹ D. VANNEROM,⁶⁰ J. VAN SANTEN ²⁸ J. VARA,⁶⁴
 J. VEITCH-MICHAELIS,¹⁰ M. VENUGOPAL,⁵⁰ M. VEREECKEN,⁶³ S. VERPOEST ³³ D. VESKE,⁸¹ A. VIJAI,¹⁴ C. WALCK,⁷²
 A. WANG ⁵² C. WEAVER ⁵ P. WEIGEL,⁶⁰ A. WEINDL,⁵⁰ J. WELDERT,⁴ A. Y. WEN,³⁵ C. WENDT ¹⁰
 J. WERTHEBACH,³² M. WEYRAUCH,⁵⁰ N. WHITEHORN ⁵ C. H. WIEBUSCH ³⁷ D. R. WILLIAMS,⁴⁹ L. WITTHAUS ³²
 A. WOLF,³⁷ M. WOLF ⁴⁰ G. WREDE,⁶⁵ X. W. XU,⁶⁹ J. P. YANEZ,⁷⁹ E. YILDIZCI,¹⁰ S. YOSHIDA ⁶⁸ R. YOUNG,⁴⁸
 S. YU ³⁶ T. YUAN ¹⁰ Z. ZHANG,⁵⁷ P. ZHELNIN,³⁵ P. ZILBERMAN,¹⁰ M. ZIMMERMAN¹⁰

ICECUBE COLLABORATION

¹Instituto de Física, Universidad Nacional Autónoma de México, Ciudad de Mexico, Mexico²Universidad Autónoma de Chiapas, Tuxtla Gutiérrez, Chiapas, México³Universidad Michoacana de San Nicolás de Hidalgo, Morelia, Mexico⁴Dept. of Physics, Pennsylvania State University, University Park, PA 16802, USA⁵Department of Physics and Astronomy, Michigan State University, East Lansing, MI, USA⁶Instituto de Astronomía, Universidad Nacional Autónoma de México, Ciudad de México, Mexico⁷Instituto Nacional de Astrofísica, Óptica y Electrónica, Puebla, Mexico⁸Institute of Nuclear Physics Polish Academy of Sciences, PL-31342 IFJ-PAN, Krakow, Poland⁹Facultad de Ciencias Físico Matemáticas, Benemérita Universidad Autónoma de Puebla, Puebla, Mexico¹⁰Dept. of Physics and Wisconsin IceCube Particle Astrophysics Center, University of Wisconsin—Madison, Madison, WI 53706, USA¹¹Departamento de Física, Centro Universitario de Ciencias Exactas e Ingenierías, Universidad de Guadalajara, Guadalajara, Mexico¹²Max-Planck Institute for Nuclear Physics, 69117 Heidelberg, Germany¹³Department of Physics, Stanford University: Stanford, CA 94305-4060, USA¹⁴Department of Physics, University of Maryland, College Park, MD, USA¹⁵Instituto Tecnológico y de Estudios Superiores de Monterrey - Campus Toluca: Toluca de Lerdo, Estado de México, MX¹⁶Department of Physics, Michigan Technological University, Houghton, MI, USA¹⁷Physics Division, Los Alamos National Laboratory, Los Alamos, NM, USA¹⁸Tsung-Dao Lee Institute & School of Physics and Astronomy, Shanghai Jiao Tong University, Shanghai, China

- ¹⁹ *Universidad Politécnica de Pachuca, Pachuca, Hgo, Mexico*
- ²⁰ *Natural Science Research Institute, University of Seoul, Seoul, Republic of Korea*
- ²¹ *Centro de Investigación en Computación, Instituto Politécnico Nacional, México City, México.*
- ²² *Dept of Physics and Astronomy, University of New Mexico, Albuquerque, NM, USA*
- ²³ *Universidad Autónoma del Estado de Hidalgo, Pachuca, Mexico*
- ²⁴ *Department of Physics, Temple University, Philadelphia, Pennsylvania, USA*
- ²⁵ *Instituto de Ciencias Nucleares, Universidad Nacional Autónoma de Mexico, Ciudad de Mexico, Mexico*
- ²⁶ *Department of Physics, Sungkyunkwan University, Suwon 16419, South Korea*
- ²⁷ *Department of Physics, Loyola University Chicago, Chicago, IL 60660, USA*
- ²⁸ *Deutsches Elektronen-Synchrotron DESY, Platanenallee 6, D-15738 Zeuthen, Germany*
- ²⁹ *Dept. of Physics and Astronomy, University of Canterbury, Private Bag 4800, Christchurch, New Zealand*
- ³⁰ *Université Libre de Bruxelles, Science Faculty CP230, B-1050 Brussels, Belgium*
- ³¹ *Niels Bohr Institute, University of Copenhagen, DK-2100 Copenhagen, Denmark*
- ³² *Dept. of Physics, TU Dortmund University, D-44221 Dortmund, Germany*
- ³³ *Bartol Research Institute and Dept. of Physics and Astronomy, University of Delaware, Newark, DE 19716, USA*
- ³⁴ *Department of Physics, Marquette University, Milwaukee, WI 53201, USA*
- ³⁵ *Department of Physics and Laboratory for Particle Physics and Cosmology, Harvard University, Cambridge, MA 02138, USA*
- ³⁶ *Department of Physics and Astronomy, University of Utah, Salt Lake City, UT 84112, USA*
- ³⁷ *III. Physikalisches Institut, RWTH Aachen University, D-52056 Aachen, Germany*
- ³⁸ *Physics Department, South Dakota School of Mines and Technology, Rapid City, SD 57701, USA*
- ³⁹ *Dept. of Physics and Astronomy, University of California, Irvine, CA 92697, USA*
- ⁴⁰ *Physik-department, Technische Universität München, D-85748 Garching, Germany*
- ⁴¹ *Dept. of Physics, University of California, Berkeley, CA 94720, USA*
- ⁴² *Dept. of Astronomy, Ohio State University, Columbus, OH 43210, USA*
- ⁴³ *Dept. of Physics and Center for Cosmology and Astro-Particle Physics, Ohio State University, Columbus, OH 43210, USA*
- ⁴⁴ *Fakultät für Physik & Astronomie, Ruhr-Universität Bochum, D-44780 Bochum, Germany*
- ⁴⁵ *Dept. of Physics and Astronomy, Uppsala University, Box 516, SE-75120 Uppsala, Sweden*
- ⁴⁶ *Dept. of Physics and Astronomy, University of Rochester, Rochester, NY 14627, USA*
- ⁴⁷ *Dipartimento di Fisica e Astronomia Galileo Galilei, Università Degli Studi di Padova, I-35122 Padova PD, Italy*
- ⁴⁸ *Dept. of Physics and Astronomy, University of Kansas, Lawrence, KS 66045, USA*
- ⁴⁹ *Dept. of Physics and Astronomy, University of Alabama, Tuscaloosa, AL 35487, USA*
- ⁵⁰ *Karlsruhe Institute of Technology, Institute for Astroparticle Physics, D-76021 Karlsruhe, Germany*
- ⁵¹ *Institute of Physics, University of Mainz, Staudinger Weg 7, D-55099 Mainz, Germany*
- ⁵² *School of Physics and Center for Relativistic Astrophysics, Georgia Institute of Technology, Atlanta, GA 30332, USA*
- ⁵³ *Department of Physics, University of Adelaide, Adelaide, 5005, Australia*
- ⁵⁴ *Dept. of Physics, Drexel University, 3141 Chestnut Street, Philadelphia, PA 19104, USA*
- ⁵⁵ *Department of Physics & Astronomy, University of Nevada, Las Vegas, NV 89154, USA*
- ⁵⁶ *Nevada Center for Astrophysics, University of Nevada, Las Vegas, NV 89154, USA*
- ⁵⁷ *Dept. of Physics and Astronomy, Stony Brook University, Stony Brook, NY 11794-3800, USA*
- ⁵⁸ *Department of Physics, Sungkyunkwan University, Suwon 16419, Republic of Korea*
- ⁵⁹ *Institute of Basic Science, Sungkyunkwan University, Suwon 16419, Republic of Korea*
- ⁶⁰ *Dept. of Physics, Massachusetts Institute of Technology, Cambridge, MA 02139, USA*
- ⁶¹ *Vrije Universiteit Brussel (VUB), Dienst ELEM, B-1050 Brussels, Belgium*
- ⁶² *Dept. of Astronomy and Astrophysics, Pennsylvania State University, University Park, PA 16802, USA*
- ⁶³ *Centre for Cosmology, Particle Physics and Phenomenology - CP3, Université catholique de Louvain, Louvain-la-Neuve, Belgium*
- ⁶⁴ *Institut für Kernphysik, Westfälische Wilhelms-Universität Münster, D-48149 Münster, Germany*
- ⁶⁵ *Erlangen Centre for Astroparticle Physics, Friedrich-Alexander-Universität Erlangen-Nürnberg, D-91058 Erlangen, Germany*
- ⁶⁶ *Dept. of Physics, University of Wuppertal, D-42119 Wuppertal, Germany*
- ⁶⁷ *Karlsruhe Institute of Technology, Institute of Experimental Particle Physics, D-76021 Karlsruhe, Germany*
- ⁶⁸ *Dept. of Physics and The International Center for Hadron Astrophysics, Chiba University, Chiba 263-8522, Japan*
- ⁶⁹ *Dept. of Physics, Southern University, Baton Rouge, LA 70813, USA*
- ⁷⁰ *Institute of Physics, Academia Sinica, Taipei, 11529, Taiwan*
- ⁷¹ *Institut für Physik, Humboldt-Universität zu Berlin, D-12489 Berlin, Germany*
- ⁷² *Oskar Klein Centre and Dept. of Physics, Stockholm University, SE-10691 Stockholm, Sweden*
- ⁷³ *Dept. of Astronomy, University of Wisconsin—Madison, Madison, WI 53706, USA*
- ⁷⁴ *Lawrence Berkeley National Laboratory, Berkeley, CA 94720, USA*
- ⁷⁵ *Dept. of Physics, Chung-Ang University, Seoul 06974, Republic of Korea*

⁷⁶*Dept. of Physics, Engineering Physics, and Astronomy, Queen's University, Kingston, ON K7L 3N6, Canada*

⁷⁷*CTSPS, Clark-Atlanta University, Atlanta, GA 30314, USA*

⁷⁸*Dept. of Physics, University of Texas at Arlington, 502 Yates St., Science Hall Rm 108, Box 19059, Arlington, TX 76019, USA*

⁷⁹*Dept. of Physics, University of Alberta, Edmonton, Alberta, T6G 2E1, Canada*

⁸⁰*Département de physique nucléaire et corpusculaire, Université de Genève, CH-1211 Genève, Switzerland*

⁸¹*Columbia Astrophysics and Nevis Laboratories, Columbia University, New York, NY 10027, USA*

⁸²*Dept. of Physics, Yale University, New Haven, CT 06520, USA*

⁸³*Department of Physics, Mercer University, Macon, GA 31207-0001, USA*

⁸⁴*Dept. of Physics and Astronomy, University of Gent, B-9000 Gent, Belgium*

⁸⁵*Dept. of Physics and Astronomy, University of Alaska Anchorage, 3211 Providence Dr., Anchorage, AK 99508, USA*

⁸⁶*Dept. of Physics, University of Oxford, Parks Road, Oxford OX1 3PU, United Kingdom*

⁸⁷*Dept. of Physics, University of Wisconsin, River Falls, WI 54022, USA*

ABSTRACT

Galactic PeVatrons are sources that can accelerate cosmic rays to PeV energies. The high-energy cosmic rays are expected to interact with the surrounding ambient material or radiation, resulting in the production of gamma rays and neutrinos. To optimize for the detection of such associated production of gamma rays and neutrinos for a given source morphology and spectrum, a multi-messenger analysis that combines gamma rays and neutrinos is required. In this study, we use the Multi-Mission Maximum Likelihood framework (3ML) with IceCube Maximum Likelihood Analysis software (i3mla) and HAWC Accelerated Likelihood (HAL) to search for a correlation between 22 known gamma-ray sources from the third HAWC gamma-ray catalog and 14 years of IceCube track-like data. No significant neutrino emission from the direction of the HAWC sources was found. We report the best-fit gamma-ray model and 90% CL neutrino flux limit from the 22 sources. From the neutrino flux limit, we conclude that the gamma-ray emission from five of the sources can not be produced purely from hadronic interactions. We report the limit for the fraction of gamma rays produced by hadronic interactions for these five sources.

1. INTRODUCTION

Since the discovery of cosmic rays (CRs) more than 100 years ago (Hess 1912), but where these high-energy particles come from has not yet been well understood. The highest energy charged particles, protons and nuclei, are thought to be extraterrestrial in origin, and their spectrum can be parametrized using a power law with an index of 2.7 up to $E_{\text{CR}} \sim 3$ PeV (or the “knee” in the spectrum), above which the spectrum steepens (Abbasi et al. 2018). The CRs below the knee are thought to originate from sources within the Milky Way galaxy, hinting at the presence of PeV hadron accelerators within the galaxy known as Galactic PeVatrons (Gabici & Aharonian 2007). Galactic PeVatrons are expected to accelerate particles up to PeV energies through Fermi acceleration and these accelerated particles are expected to be confined within the Milky Way galaxy (Abbasi et al. 2018).

Supernova remnants (SNRs) are a potential class of Galactic PeVatrons. The particles are accelerated by diffusive shock acceleration in the expanding shock. Only 10% of the energy of SNRs is needed to explain the observed CR energy density in the Galaxy (Blandford & Ostriker 1978). For the most energetic galactic CRs, it is assumed that only young SNRs can accelerate CRs beyond 100 TeV (Bell et al. 2013). The accelerated CRs can escape the SNR and diffuse into the surrounding interstellar medium. They can interact with the surrounding material like molecular clouds and produce charged and neutral pions. Therefore, young SNRs located near star clusters or molecular clouds are thought to be bright in gamma rays due to hadronic interactions. High-energy gamma rays and neutrinos can be efficiently produced by the decay of charged and neutral pions. Other potential source classes of Galactic PeVatrons include young massive star clusters, YMCs (Bykov et al. 2020) and pulsar wind nebulae, PWNe (Di Palma et al. 2017).

TeV gamma rays can also be produced by leptonic interactions such as inverse Compton scattering. However, inverse Compton scattering is strongly suppressed at energies above 50 TeV (Hinton & Hofmann 2009) due to the Klein-Nishina effect (Klein & Nishina 1929). On the other hand, the gamma rays produced by neutral pion decays are not suppressed

* also at Institute of Physics, Sachivalaya Marg, Sainik School Post, Bhubaneswar 751005, India

† also at Department of Space, Earth and Environment, Chalmers University of Technology, 412 96 Gothenburg, Sweden

‡ also at Earthquake Research Institute, University of Tokyo, Bunkyo, Tokyo 113-0032, Japan

at O(10 TeV), making TeV gamma-ray emitters excellent candidates for Galactic PeVatrons. Moreover, high-energy neutrinos are also produced in hadronic interactions via charged pion decays and their detection is evidence of hadron acceleration. Because of this relationship, a joint search using TeV gamma-ray and neutrino data from known TeV gamma-ray emitters can test whether a source is a Galactic PeVatron.

Several potential Galactic PeVatrons have been investigated by the community. The HAWC collaboration reported that the TeV gamma-ray spectrum of HAWC J1825-134 extends up to 200 TeV without any cut-off, much higher than the Klein-Nishina suppression energy (Albert et al. 2021). This may indicate hadronic acceleration. The HAWC collaboration also reported HAWC J2227+610 as a potential PeVatron candidate from TeV gamma-ray observations and concluded the proton cutoff energy is at least 800 TeV (Albert et al. 2020a). The HAWC collaboration studied the ultra-high-energy spectrum off MGRO J1908+06 and their model allows a hadronic component at the highest energy (Albert et al. 2022). The HESS Collaboration reported evidence of a PeVatron at the galactic center based on gamma-ray observations up to 40 TeV (Abramowski et al. 2016).

The IceCube Neutrino Observatory has previously searched for neutrino emission from galactic sources, both individual sources and classes of sources. Abbasi et al. (2023a) searched for neutrino emission from LHAASO’s first catalog of sources with energy above 100 TeV (Cao et al. 2021) using a fixed spatial extension and a power law spectrum. They found no significant emission, neither from single sources nor from stacked catalogs of SNRs and PWNe. Recently, IceCube has detected neutrinos from the galactic plane (Abbasi et al. 2023b). The observation was made using a neutrino detection channel, cascades, which has relatively large angular uncertainty. Therefore, IceCube could not distinguish between diffuse emission in the galactic plane and a collection of individual sources. The IceCube collaboration also searched the entire galactic plane and regions near TeV gamma-ray sources using an extended source hypothesis and a power law spectrum, finding no significant neutrino emission (Abbasi et al. 2023c). However, these searches have not directly incorporated gamma-ray data. The simultaneous use of both data sets incorporates more physically motivated spectra and provides a direct constraint on the hadronic ratio, i.e. the fraction of gamma rays originating from hadronic interactions.

If the gamma rays and neutrinos originate from hadronic interactions, the spectra of the gamma rays and neutrinos have a fixed relationship. In the case of Galactic PeVatrons, the proton-proton (pp) interaction is expected to be dominant as compared to the photo-hadronic interactions (Ahlers & Murase 2014). In the pp interactions, protons interact with nearby material and produce charged and neutral pions. The ratio between the production of charged and neutral pions is about 2:1. Charged pions decay further into three neutrinos and other products, with each resulting neutrino having about a quarter of the energy of the charged pion. The neutral pions decay into two gamma rays, each with half of the energy of the neutral pion, on average. Therefore, we expect that for charged and neutral pion decay, the energy of the neutrino produced will be half the energy of the gamma-ray produced on average. On Earth, the observed flux is

$$E_\gamma J_\gamma(E_\gamma) \approx e^{\frac{-d}{\lambda_{\gamma\gamma}}} \frac{1}{3} \sum_{\nu_\alpha} E_\nu J_{\nu_\alpha}(E_\nu) \quad (1)$$

where $J_{\nu_\alpha}(E_\nu)$ is the neutrino differential particle flux with the neutrino flavor α , d is the distance to the source, $\lambda_\gamma(E_\gamma)$ is the interaction length of the gamma ray and $J_\gamma(E_\gamma)$ is the gamma-ray differential particle flux (Ahlers & Murase 2014). Since we only consider galactic sources, we assume that the absorption of gamma-rays is negligible ($\frac{-d}{\lambda_{\gamma\gamma}} \approx 0$) and the flux from each neutrino flavor is the same due to oscillations. The relationship between the gamma-ray flux (J_γ) and the muon neutrino flux (J_{ν_μ}) is thus

$$J_{\nu_\mu}(E_{\nu_\mu}) = 2J_\gamma(2E_{\nu_\mu}). \quad (2)$$

Therefore, if the gamma rays from a galactic source originate from hadronic interactions, the neutrino counterpart should exhibit the same morphology and have the same spectral shape shifted to lower energies. This relationship is used in this work to model and simultaneously fit the gamma-ray and neutrino data.

2. INSTRUMENTS AND DATASETS

2.1. HAWC Gamma-ray Observatory

The High Altitude Water Cherenkov (HAWC) Observatory is located near Sierra Negra, Mexico, at a latitude of $19^\circ N$ and an altitude of 4100 m. It has been in continuous operation since November 2014 (Abeysekara et al. 2023). The observatory consists of 300 Water Cherenkov Detectors (WCDs), covering an area of 22000 m². Each WCD

consists of a steel tank 7.3 m in diameter and 5.4 m high, lined with a plastic bladder and filled with purified water. At the bottom of the water tank, three 8-inch photomultiplier tubes (PMTs) are arranged in an equilateral triangle with a side length of 3.2m, and with one 10-inch PMT in the center (Abeysekara et al. 2023).

When high-energy gamma rays interact with the Earth’s atmosphere, they create a cascade of particles called an extensive air shower (EAS). When these particles reach the HAWC detector and pass through the water at a speed greater than the speed of light in water, Cherenkov light is induced and collected by the PMTs in the WCDs. HAWC uses the observed Cherenkov emission to reconstruct the properties of the primary gamma rays.

HAWC divides the detected shower events into a 2D array of analysis bins based on the fraction of triggered PMTs during a shower event and the reconstructed energy of the event (Abeysekara et al. 2019a). The events within an analysis bin are expected to have similar characteristics, including angular resolution, primary gamma-ray energy, and gamma-to-hadron likelihood (signal-to-noise ratio), which allows HAWC to perform a binned likelihood analysis.

In this study, we use 2141 days of HAWC data using the Pass 5 reconstruction (Yun-Carcamo et al. 2023). The event-related energy is estimated using the “ground parameter” estimator described in Abeysekara et al. (2019a). This energy estimator uses the charge at a fixed optimal distance from the shower axis to estimate the energy. The dataset covers the period from June 15, 2015 to October 21, 2021 with a livetime of more than 90%.

2.2. The IceCube Neutrino Observatory

The IceCube Neutrino Observatory is a neutrino detector located at the geographic South Pole (Aartsen et al. 2017). The primary IceCube detector comprises a cubic kilometer array of 5160 digital optical modules (DOMs). These DOMs are arranged along 86 readout and support cables, called strings, embedded in the glacial ice at depths between 1.45 km and 2.45 km. Each DOM consists of a 10-inch PMT and its readout electronics and is housed in a pressure-resistant sphere (Abbasi et al. 2009). DOMs are designed to detect the Cherenkov light produced by charged particles moving through the ice (Abbasi et al. 2010). These particles originate from the charged-current (CC) interactions or neutral-current (NC) interactions of all flavors of neutrinos. IceCube events are typically divided into two categories: track-like events produced by CC interactions of muon neutrinos and cascade-like events from all other CC interactions and NC interactions. The DOMs record the Cherenkov light, allowing events to be classified and event properties, such as the direction of the incident neutrinos and the deposited energy, to be reconstructed (Aartsen et al. 2014).

The dataset used in this analysis includes 14 years of IceCube track-like data from April 6, 2008 to May 23, 2022. Track-like data provide a better angular resolution ($\sim 1^\circ$ angular uncertainty for a typical \sim TeV neutrino) compared to cascade-like events. This makes track-like events more suited to search for sources with an extension below a few degrees. The data from April 6, 2008 to May 13, 2011 were taken with the partially constructed detector with 40, 59, and 79 strings (IC40, IC59, and IC79), with each configuration spanning approximately one year (Aartsen et al. 2014). The remaining data were recorded with the full detector configuration with 86 strings (IC86).

3. ANALYSIS METHOD

3.1. Source selection

HAWC detected 65 sources with a significance above 5σ in the third HAWC catalog (3HWC) (Albert et al. 2020b) using 1523 days of data. The 3HWC provides the location and the gamma-ray flux at a pivot energy of 7 TeV for each source in the catalog. The pivot energy E_0 is the energy of normalization of the spectral function, which is specified in terms of E/E_0 . If the gamma-ray emission from these sources comes from hadronic interactions, the neutrino flux will be described by the same spectral function with half the pivot energy (3.5 TeV), according to Equation 2. We calculate the IceCube 90% confidence level (CL) sensitivity for a point source with an E^{-2} unbroken power law spectrum. The sensitivity is defined as the median expected 90% CL upper limit. The sensitivity can be determined using background trials and signal trials. Background trials are done by performing the analysis using simulated data obtained by scrambling real data in right ascension (RA). Scrambling data as background does not suffer from systematic uncertainties and therefore is a robust way to generate background trials. Signal trials are generated by scrambling data and adding signal using simulation data. The calculation of sensitivity is based on a maximum likelihood method as used in the IceCube 10-year search for neutrino sources (Aartsen et al. 2020a). In this work, we use a new likelihood analysis software component called i3mla (Abbasi et al. 2021) with the multi-mission maximum likelihood framework (3ML) (Vianello et al. 2017). Details of i3mla are described in section 3.4. The likelihood consists of a spatial term and an energy term, as explained in more detail in Appendix A.

We select sources whose predicted neutrino flux from hadronic interactions is larger than the sensitivity of the IceCube E^{-2} point source search. The hard E^{-2} spectrum is an optimistic choice made to avoid missing any potential sources in our source selection step. The final sensitivity of the joint search will change depending on the best-fit gamma-ray spectrum and spatial extension. The sensitivity of IceCube and the predicted neutrino flux from 3HWC sources are shown in Figure 1. We exclude two extra-galactic sources, Markarian 421 and Markarian 501, as this study focuses on galactic sources. We also exclude four sources classified as secondary sources in 3HWC, as these are likely to be statistical fluctuations near bright sources. Our final source list comprises 22 sources from 3HWC. Many of the sources are still unidentified but some have potential associations with pulsar wind nebulae, supernova remnants, and star-forming regions.

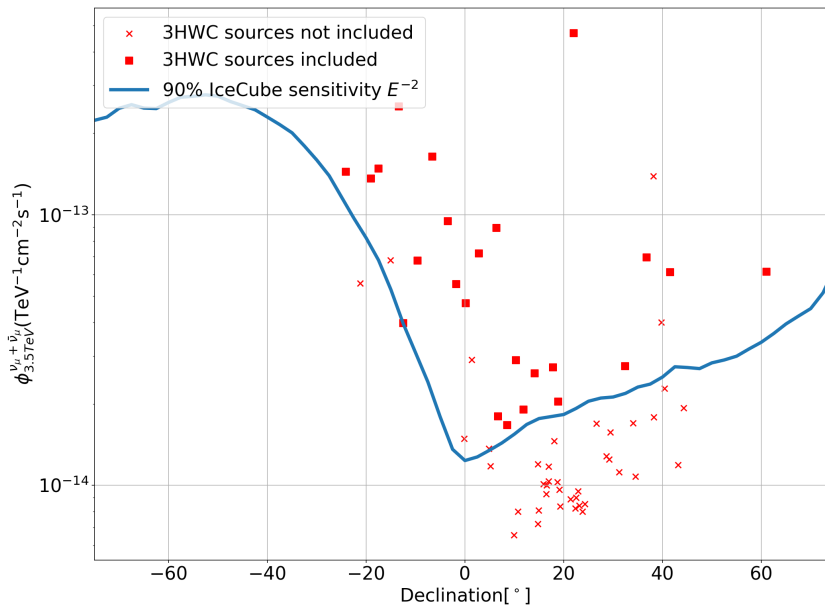


Figure 1. The IceCube E^{-2} time-integrated point source sensitivity as a function of source declination. The x-axis is the declination in degrees and the y-axis is the differential neutrino flux ($\text{TeV}^{-1}\text{cm}^{-2}\text{s}^{-1}$) at pivot energy $E_0 = 3.5$ TeV. Each red cross and red square represents the predicted neutrino flux of a 3HWC source assuming all the gamma rays from the sources originated from proton-proton hadronic interaction. Galactic 3HWC sources (excluding 3HWC secondary sources) with a predicted neutrino flux above the IceCube sensitivity are included in our source list and shown as red squares.

3.2. Model selection and fit using gamma-ray data

To obtain a spatial and spectral model for the joint analysis of the sources, we first fit each gamma-ray source with an updated HAWC data set. We use 2141 days of HAWC ground parameter energy estimator maps with the Pass 5 reconstruction for our model selection procedure. The dataset contains more data and a better energy estimator compared to the dataset used in 3HWC. The new reconstruction provides a better angular reconstruction and gamma/hadron separation. We use the 3ML framework (Vianello et al. 2017) with the HAWC Accelerated Likelihood (HAL) plugin (Abeysekara et al. 2021) for our model selection and model fitting. HAL is a Python-based, maximum likelihood software module designed to perform HAWC analysis using a binned likelihood. In conjunction with 3ML, it can perform both stand-alone HAWC analyses and joint analyses with other experiments. We select the model that best describes the gamma-ray emission based on the log-likelihood (LLH). We use the position in 3HWC as a starting point for our initial fit. First, we use a simple power law and a point source as spectral and spatial hypotheses. The simple power law is parameterized as $\frac{dN_\gamma}{dE_\gamma} = \phi \left(\frac{E_\gamma}{7\text{TeV}}\right)^\alpha$, where ϕ is the flux normalization and α is the spectral index. The free parameters in this model are the Right Ascension (RA), the Declination (Dec), the spectral index, and the gamma-ray flux. Second, we test the extended source hypothesis, where we fix the RA and Dec of the

source to the best-fit values and fit for a Gaussian extension along with the spectral index and flux. We accept the extended source hypothesis if twice the difference between the log-likelihood ($2\Delta LLH$) of the two models (point source hypothesis and extended source hypothesis) is greater than 16, corresponding to 4σ according to Wilks' theorem (Wilks 1938). Finally, we test the spectrum curvature hypothesis, where we fixed the RA, Dec, and extension (if the source is extended) and we use a log-parabola spectrum to fit the data again. The log-parabola spectrum is parameterized by

$$\frac{dN_\gamma}{dE_\gamma} = \phi \cdot \left(\frac{E_\gamma}{7\text{TeV}}\right)^{\alpha - \beta \cdot \log \frac{E_\gamma}{7\text{TeV}}} \quad (3)$$

The free parameters in this model are α , β and the gamma-ray flux at 7 TeV. We accept the spectral curvature hypothesis if the $2\Delta LLH$ between the spectral curvature hypothesis and the power law hypothesis is greater than 16. Based on the results of these fits, we obtain the final model that contains information about the morphology and spectrum of the source.

3.3. IceCube likelihood with i3mla

Combining IceCube neutrino data with the HAWC gamma-ray data is a non-trivial task because of the complexity of the instrument response functions and the likelihood calculation. We use a Python-based maximum likelihood module called i3mla (Abbasi et al. 2021) for IceCube likelihood calculation. Similar to HAL, i3mla is specifically designed to be compatible with the 3ML framework. i3mla uses instrument response functions (IRFs) to encapsulate the detector properties and performances of the detector determined from Monte Carlo simulations. The IRFs then can be used to calculate the energy likelihood of IceCube. This differs from other IceCube analysis software that pre-computes the energy likelihood for an assumed spectrum, e.g. a simple power law, and uses all the Monte Carlo data for the energy likelihood calculation. The new tabulated IRFs method speeds up the likelihood computation process when fitting for an arbitrary spectrum, making it possible to fit any spectral parameters during the model fitting in i3mla.

In this analysis, we use spatial and energy likelihood terms to calculate the likelihood of the model. The signal hypothesis assumes some neutrino emission from the source of interest. The background hypothesis assumes all non-neutrino events and neutrino events originate from atmospheric muons, atmospheric neutrinos, and astrophysical neutrinos that are not associated with the source. We model the IceCube point spread function (PSF) as a 2D Gaussian and the angular error of the 2D Gaussian is estimated during the reconstruction. The signal spatial likelihood is the PSF convolved with the morphology of the source and the signal energy likelihood is calculated using the IRFs and the model spectrum. The background spatial likelihood is estimated from the data by binning the data in reconstructed declination and creating a spline using the resulting histogram. The background spatial likelihood is a function of declination only. The background energy likelihood is estimated from the data by weighting the simulation using the spectral hypothesis and binning it in reconstructed declination and energy. The method is conceptually identical to the previous IceCube 10-year time-integrated point source search in Aartsen et al. (2020a) and the extended source search in Abbasi et al. (2023a,c). A detailed description of the likelihood can be found in Appendix A.

3.4. Joint fit with Gamma rays and Neutrinos

After obtaining a spatial and spectral model for each source, we perform a joint fit with HAWC gamma-ray data and IceCube neutrino data. We keep the location and extension of the model fixed. We add a neutrino component to the model that coincides with the gamma-ray source. We connect the neutrino and gamma-ray emission spectral parameters according to the relation in Equation 2 and allow them to float during the fit. We let the flux normalization of the neutrino and gamma-ray components float independently. Table 1 shows the properties of the model parameters.

To calculate the p-value, we perform a large number of background trials by scrambling the IceCube data in RA and building the background test statistic (TS) distribution (Aartsen et al. 2020b). This is done to avoid any dependence on the simulation when testing for a neutrino source. The calculation of the IceCube component of the likelihood is fast. However, using raw HAWC binned maps for computing the HAWC component of the likelihood is prohibitively computationally expensive for such a large number of trials. Therefore, the HAWC data are fixed during the background scrambling process so that we can pre-compute the HAWC component of the likelihood. We extract the HAWC likelihood around the best-fit spectral parameters and save it into a table. Since the location and extension are fixed during the fit, we do not extract the likelihood around the spatial parameters. For spectral parameters, we evaluate the HAWC likelihood within $\pm 5\sigma$ of the best-fit spectral shape parameters while maximizing it over the flux normalization.

Since the gamma-ray and neutrino fluxes are floated independently, maximizing the likelihood over the gamma-ray flux normalization leads to a maximum likelihood for HAWC at the spectral shape parameters in the joint fit. For a

Model parameters	Gamma-ray spectrum	Neutrino spectrum	Relation
Right ascension(RA)	Fix	Fix	Equal
Declination(dec)	Fix	Fix	Equal
Extension	Fix	Fix	Equal
α	Float	Float	Equal
β	Float	Float	Equal
Pivot energy	Fix	Fix	Neutrino pivot energy = Gamma-ray pivot energy / 2
Flux normalization	Float	Float	Independent

Table 1. Table summarizing the model parameters of the Gamma-ray and Neutrino components and their relations. Parameters listed as fix will be fixed during model fitting and parameters listed as float will be fitted during model fitting.

log-parabola spectrum, there are two free parameters for the spectral shape (α and β), and we use a 50×50 grid around the best-fit parameters for the likelihood evaluation. For a power-law spectrum, there is only one free parameter for the spectral shape (α) and we evaluate 300 points around the best-fit parameters. We have developed a new custom plugin for 3ML to read the likelihood table and construct a spline. The 3ML plugin returns the spline value for the likelihood evaluation. This method speeds up the likelihood calculation because the program does not have to calculate the HAWC likelihood for each pixel and each bin during the fitting. Figure 2 shows an example of the likelihood.

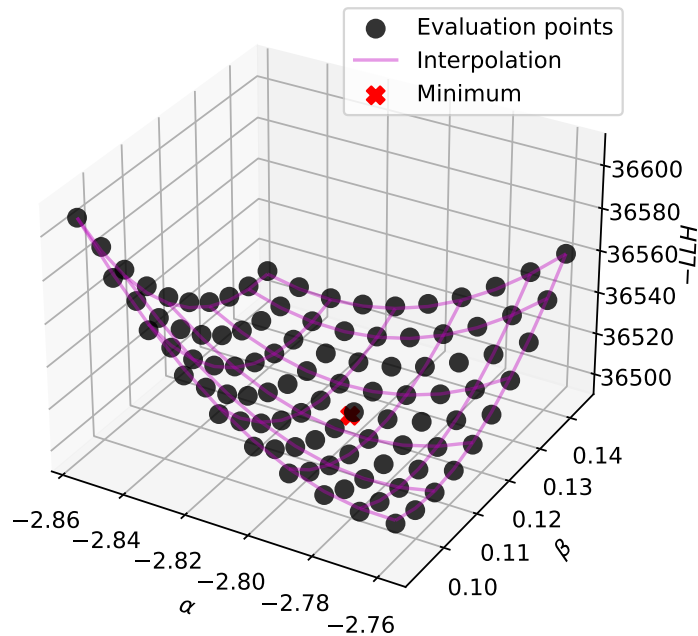


Figure 2. A plot visualizing the HAWC likelihood for an example source. The y axis is the negative LLH. The negative LLH is evaluated around the best-fit model. For a log-parabola spectrum, we evaluate 50 points within $\pm 5\sigma$ for α and β around the minimum. For a power-law spectrum, we evaluate 300 points for spectral index within $\pm 5\sigma$. The negative log-likelihood was minimized over the gamma-ray flux for each point.

The background TS distribution is calculated by generating 50,000 background-only trials. For each background trial, the IceCube data are scrambled in RA while keeping the HAWC component of the likelihood unchanged, and the joint analysis is performed. To determine the sensitivity to the neutrino flux of the joint search, we inject different

simulated values of the neutrino flux at the location of the best-fit gamma-ray source with its best-fit extension and spectral shape. The 90% CL sensitivity is the neutrino flux required for the TS to exceed the median of the background-only TS distribution 90% of the time. The 5σ discovery potential is the neutrino flux required for the TS to exceed the 5σ fluctuation of the background-only TS distribution 50% of the time. Figure 3 shows the ratio between the sensitivity and the predicted neutrino flux assuming pp interactions, as well as the ratio between the 5σ discovery potential and the predicted neutrino flux assuming pp interactions.

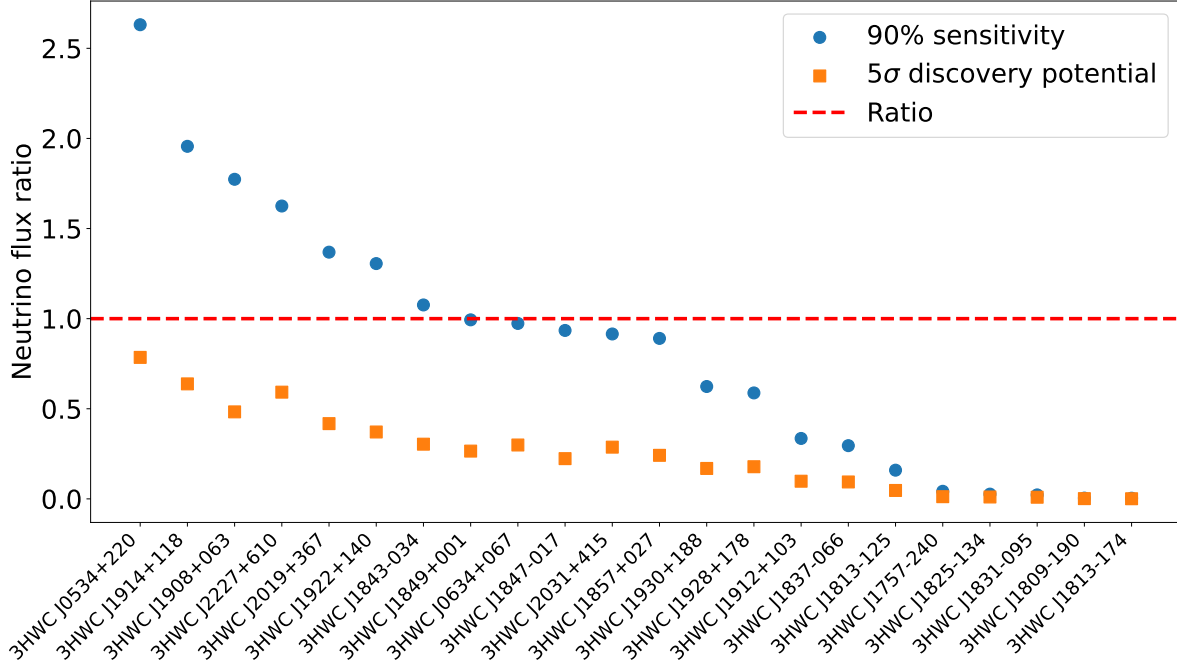


Figure 3. The ratio between the predicted neutrino flux and the sensitivity (blue dot) and 5σ discovery potential (orange rectangle) of the analysis. The sources above the red dashed line are the sources that are likely to be detected by IceCube if they are hadronic sources. The plot is ordered by the sensitivity ratio.

We derive the pre-trial p-value for each source by using the background TS distribution of each source. The pre-trial p-value is the percentage of background trials having a TS higher than the TS of the actual search. To correct for the look-elsewhere effect, we create a pre-trial p-value distribution by searching for neutrinos from each source using the same background data and picking the smallest p-value from the 22 sources in each background trial. The post-trial p-value is the fraction of p-values in the aforementioned distribution that are smaller than the smallest pre-trial p-value in the data. With this method, the correlations between different sources can be correctly taken into account.

In addition to searching for individual sources, we perform a binomial test to determine whether a subset of the sources has TS values inconsistent with the background (Abbasi et al. 2022a). The test statistic of the binomial test, $p_{binomial}$, is the minimum probability, over all k that at least k p-values are at or below the k th smallest p-value observed, p_k :

$$p_{binomial} = \min_k P_k = \min_k \sum_{m=k}^N \binom{N}{m} p_k^m (1 - p_k)^{N-m} \quad (4)$$

To account for the look-elsewhere effect, we create a distribution of $p_{binomial}$ by performing the binomial test on scrambled data. We compute the post-trial p-value of the binomial test using the $p_{binomial}$ value for data. To calculate the overall post-trial p-value accounting for the trials from doing two searches, we create another p-value distribution by choosing, for each background trial, the smaller of the post-trial p-values from the individual source search and the

binomial test. This method takes into account the correlation between the individual source search and the binomial test. We then compare the smaller of the two p-values from data with this distribution to obtain the overall p-value.

4. RESULTS

4.1. HAWC best-fit result

First, we present the best-fit results for the gamma-ray emission from the HAWC Pass 5 data alone. Table 2 summarizes the best-fit location, extension, and spectral parameters of each source in our list. In addition, we report the statistical and systematic uncertainty of the spectral fit results. Systematic uncertainties of the HAWC detector include PMT efficiency, charge uncertainty, etc., and are described in [Abeysekara et al. \(2019b\)](#). To evaluate their effect, we perform the model selection using samples simulated with different settings and compare the results with the baseline simulation. The errors of each type of systematic uncertainty are added in quadrature to obtain the total systematic uncertainty, which is given in the table 2.

Name	RA [°]	Dec [°]	Ext [°]	α	β	F_7 [$10^{-14}\text{TeV}^{-1}\text{cm}^{-2}\text{s}^{-1}$]	Nearest TeVCat source
3HWC J0534+220	83.64	22.01	PS	$-2.82^{+0.01}_{-0.01} +^{+0.09}_{-0.03}$	$0.12^{+0.01}_{-0.01} +^{+0.0}_{-0.05}$	$23.82^{+0.23}_{-0.22} +^0_{-2.7}$	Crab
3HWC J0634+067	98.59	6.66	0.49	$-2.57^{+0.1}_{-0.1} +^{+0.21}_{-0.0}$	0	$1.35^{+0.43}_{-0.32} +^0_{-2.6}$	HAWC J0635+070
3HWC J1757-240	269.32	-23.86	PS	$-2.58^{+0.26}_{-0.26} +^{+0.97}_{-0.11}$	0	$1.68^{+1.03}_{-0.66} +^0_{-1.5}$	HESS J1800-240B
3HWC J1809-190	272.42	-19.34	0.23	$-2.09^{+0.15}_{-0.15} +^{+0.01}_{-0.27}$	$0.23^{+0.07}_{-0.02} +^{+0.0}_{-0.3}$	$11.69^{+1.11}_{-1.06} +^0_{-3.1}$	HESS J1809-193
3HWC J1813-125	273.4	-12.7	0.27	$-2.6^{+0.08}_{-0.08} +^{+0.48}_{-0.0}$	0	$2.87^{+0.47}_{-0.44} +^{+1.0}_{-0}$	HESS J1813-126
3HWC J1813-174	273.4	-17.74	0.26	$-1.91^{+0.16}_{-0.15} +^{+0.54}_{-0.53}$	$0.35^{+0.08}_{-0.08} +^{+0.31}_{-0.31}$	$13.47^{+1.22}_{-1.07} +^{+2.5}_{-5.6}$	2HWC J1814-173
3HWC J1825-134	276.49	-13.63	0.46	$-2.45^{+0.02}_{-0.02} +^{+0.1}_{-0.02}$	$0.13^{+0.02}_{-0.02} +^{+0.0}_{-0.14}$	$41.02^{+1.12}_{-1.12} +^0_{-8.9}$	2HWC J1825-134
3HWC J1831-095	277.85	-9.85	1.14	$-2.59^{+0.03}_{-0.04} +^{+0.22}_{-0.0}$	$0.14^{+0.02}_{-0.03} +^{+0.0}_{-0.18}$	$37.37^{+2.08}_{-1.9} +^0_{-8.4}$	HESS J1831-098
3HWC J1837-066	279.38	-6.83	0.65	$-2.69^{+0.02}_{-0.02} +^{+0.14}_{-0.0}$	$0.1^{+0.01}_{-0.01} +^{+0.0}_{-0.08}$	$34.52^{+0.89}_{-0.88} +^0_{-4.8}$	2HWC J1837-065
3HWC J1843-034	280.95	-3.39	0.6	$-2.51^{+0.03}_{-0.03} +^{+0.2}_{-0.0}$	$0.13^{+0.02}_{-0.02} +^{+0.0}_{-0.21}$	$21.51^{+0.79}_{-0.74} +^0_{-8.4}$	2HWC J1844-032
3HWC J1847-017	282.07	-1.78	0.75	$-2.66^{+0.03}_{-0.03} +^{+0.28}_{-0.0}$	$0.09^{+0.02}_{-0.02} +^{+0.0}_{-0.18}$	$17.03^{+0.81}_{-0.76} +^0_{-2.7}$	HESS J1848-018
3HWC J1849+001	282.31	0.02	0.68	$-2.42^{+0.03}_{-0.04} +^{+0.22}_{-0.0}$	$0.13^{+0.02}_{-0.02} +^{+0.0}_{-0.24}$	$15.38^{+0.69}_{-0.7} +^0_{-3.9}$	IGR J18490-0000
3HWC J1857+027	284.35	2.82	0.6	$-2.73^{+0.02}_{-0.02} +^{+0.28}_{-0.0}$	$0.13^{+0.02}_{-0.02} +^{+0.0}_{-0.18}$	$16.3^{+0.59}_{-0.58} +^0_{-3.3}$	HESS J1857+026
3HWC J1908+063	287.02	6.35	0.57	$-2.44^{+0.02}_{-0.02} +^{+0.09}_{-0.01}$	$0.09^{+0.01}_{-0.01} +^{+0.0}_{-0.07}$	$20.02^{+0.52}_{-0.5} +^0_{-2.6}$	MGRO J1908+06
3HWC J1912+103	288.1	10.32	0.52	$-2.83^{+0.05}_{-0.05} +^{+0.32}_{-0.0}$	$0.14^{+0.04}_{-0.04} +^{+0.0}_{-0.16}$	$5.79^{+0.47}_{-0.44} +^{+2.2}_{-5.6}$	HESS J1912+101
3HWC J1914+118	288.71	11.79	0.71	$-2.69^{+0.04}_{-0.04} +^{+0.39}_{-0.0}$	0	$4.09^{+0.59}_{-0.5} +^0_{-2.6}$	2HWC J1914+117*
3HWC J1922+140	290.74	14.06	0.13	$-2.77^{+0.06}_{-0.05} +^{+0.12}_{-0.0}$	0	$1.37^{+0.17}_{-0.12} +^{+0.054}_{-0.071}$	W 51
3HWC J1928+178	292.13	17.81	0.83	$-2.52^{+0.04}_{-0.04} +^{+0.18}_{-0.0}$	$0.11^{+0.02}_{-0.03} +^{+0.0}_{-0.14}$	$9.4^{+0.58}_{-0.54} +^0_{-1.7}$	2HWC J1928+177
3HWC J1930+188	292.56	18.81	0.76	$-2.51^{+0.04}_{-0.04} +^{+0.12}_{-0.0}$	$0.14^{+0.03}_{-0.03} +^{+0.0}_{-0.12}$	$9.0^{+0.49}_{-0.48} +^0_{-2.2}$	SNR G054.1+00.3
3HWC J2019+367	304.9	36.77	0.32	$-2.04^{+0.05}_{-0.05} +^{+0.02}_{-0.13}$	$0.31^{+0.03}_{-0.03} +^{+0.0}_{-0.22}$	$11.7^{+0.4}_{-0.38} +^0_{-2.3}$	VER J2019+368
3HWC J2031+415	308.01	41.49	0.51	$-2.52^{+0.04}_{-0.04} +^{+0.26}_{-0.0}$	$0.19^{+0.03}_{-0.03} +^{+0.0}_{-0.28}$	$12.06^{+0.59}_{-0.56} +^0_{-3.7}$	TeV J2032+4130
3HWC J2227+610	336.82	60.94	PS	$-2.42^{+0.2}_{-0.21} +^{+0.78}_{-0.27}$	0	$1.53^{+0.68}_{-0.47} +^{+0.5}_{-1.5}$	Boomerang

Table 2. The best-fit result from the HAWC data. The columns from left to right are 3HWC source name, Right Ascension, Declination, Gaussian extension (PS indicates a point source), α and β of the log-parabola spectrum ($\beta = 0$ for power law spectrum), the differential gamma-ray flux at 7 TeV, and the nearest TeVCat source listed in 3HWC ([Albert et al. 2020b](#); [Wakely & Horan 2008](#)). The first uncertainty is statistical and the second is systematics.

4.2. Joint-fit result

We performed the joint fit using the best-fit model of HAWC and added a neutrino source as described in Section 3.4. We found no significant neutrino emission. The smallest pre-trial p-value from the individual source search is 0.07 for 3HWC J2019+367, which corresponds to a post-trial p-value of 0.21 when accounting for the trials in the individual source search. The pre-trial p-value for each source can be found in appendix B. We performed the binomial test and found no significant neutrino emission from any subset of the 22 sources. The pre-trial p-value of the binomial test is 0.09 at k=6 (3HWC J2019+367, 3HWC J2031+415, 3HWC J1912+103, 3HWC J1908+063, 3HWC J1857+027, 3HWC J1928+178) and corresponds to a post-trial p-value of 0.34 when only accounting for trials in the binomial test. Accounting for both the trials from the individual source search and the binomial test, the final post-trial p-value is 0.37.

Based on the null result of the joint search, we also calculated the neutrino flux limits at 90% CL for the 22 sources (see table 3). We account for IceCube systematics by calculating the sensitivity using different Monte Carlo systematic sets and adding the difference to the baseline in quadrature. Appendix C details the effect of IceCube systematics on the flux limit for each source. Table 3 shows the neutrino flux limit for each source. Figure 4 shows, by declination, the neutrino flux limit and the neutrino flux predicted from the best gamma-ray fit assuming all the gamma-ray emission is from hadronic interaction.

Name	RA [°]	Dec [°]	Extension [°]	Neutrino 90% CL flux limit [TeV ⁻¹ cm ⁻² s ⁻¹]	Predicted neutrino flux [TeV ⁻¹ cm ⁻² s ⁻¹]	IceCube 90% energy range [TeV]
3HWC J0534+220	83.64	22.01	PS	2.44×10^{-13}	4.74×10^{-13}	0.3 - 21.6
3HWC J0634+067	98.59	6.66	PS	5.04×10^{-14}	2.74×10^{-14}	0.4 - 143.0
3HWC J1757-240	269.32	-23.86	0.10	9.94×10^{-13}	3.35×10^{-14}	98.7 - 6870.0
3HWC J1809-190	272.42	-19.34	0.23	7.47×10^{-11}	2.32×10^{-13}	38.7 - 468.3
3HWC J1813-125	273.40	-12.70	0.27	4.42×10^{-13}	5.55×10^{-14}	41.3 - 3897.3
3HWC J1813-174	273.40	-17.74	0.26	6.33×10^{-11}	2.72×10^{-13}	9.60 - 263.5
3HWC J1825-134	276.49	-13.63	0.46	3.94×10^{-11}	8.00×10^{-13}	26.2 - 519.7
3HWC J1831-095	277.85	-9.85	1.14	4.71×10^{-11}	7.39×10^{-13}	3.1 - 229.4
3HWC J1837-066	279.38	-6.83	0.65	3.12×10^{-12}	6.91×10^{-13}	0.7 - 94.1
3HWC J1843-034	280.95	-3.39	0.60	4.71×10^{-13}	4.28×10^{-13}	0.7 - 57.0
3HWC J1847-017	282.07	-1.78	0.75	2.70×10^{-13}	3.45×10^{-13}	0.5 - 49.1
3HWC J1849+001	282.31	0.02	0.68	3.56×10^{-13}	3.08×10^{-13}	0.7 - 56.9
3HWC J1857+027	284.35	2.82	0.60	7.87×10^{-13}	3.26×10^{-13}	0.4 - 29.2
3HWC J1908+063	287.02	6.35	0.57	5.24×10^{-13}	4.00×10^{-13}	0.6 - 65.1
3HWC J1912+103	288.10	10.32	0.52	7.61×10^{-13}	1.11×10^{-13}	0.4 - 24.1
3HWC J1914+118	288.71	11.79	0.71	4.87×10^{-14}	7.93×10^{-14}	0.3 - 73.9
3HWC J1922+140	290.74	14.06	0.13	2.33×10^{-14}	2.68×10^{-14}	0.3 - 51.8
3HWC J1928+178	292.13	17.81	0.83	5.73×10^{-13}	1.85×10^{-13}	0.5 - 42.7
3HWC J1930+188	292.56	18.81	0.76	3.50×10^{-13}	1.78×10^{-13}	0.5 - 36.6
3HWC J2019+367	304.90	36.77	0.32	3.87×10^{-13}	2.34×10^{-13}	1.1 - 34.2
3HWC J2031+415	308.01	41.49	0.51	5.47×10^{-13}	2.40×10^{-13}	0.5 - 25.8
3HWC J2227+610	336.82	60.94	PS	2.51×10^{-14}	3.11×10^{-14}	0.4 - 78.4

Table 3. Neutrino 90% CL flux limit at 3.5 TeV from the individual source search. The neutrino flux limit is calculated by injecting a flux of neutrino according to the gamma-ray best-fit model’s neutrino prediction. The predicted neutrino flux is calculated from the gamma-ray fit result assuming the emission is purely hadronic. The IceCube 90% energy range is the central 90% energy range of the signal neutrinos. The smallest pre-trial p-value is 0.07 and it corresponds to 0.21 post-trial p-value after accounting for trials in the individual source search.

Five sources have a lower neutrino 90% CL flux limit than the predicted neutrino flux. In these cases, we conclude that the gamma-ray emission in the TeV range cannot completely originate from hadronic interactions. If we further assume that the leptonic component shares a similar spectral shape in the TeV energy range, we can constrain the percentage of the gamma-ray flux originating from hadronic interactions. Among these sources, 3HWC J2227+610 was studied by the HAWC collaboration and could be associated with supernova remnant G106.3+2.7. HAWC found a hint for PeV proton acceleration and suggested that 3HWC J2227+610 could be a Galactic PeVatron (Albert et al. 2020a). The Crab Nebula (3HWC J0534+220) is the brightest source in the TeV sky and is the most strongly constrained. 3HWC J1922+140 is close to the W 51 region which contains the star-forming region W51B, the supernova remnant W51C, and a potential PWN, CXOU J192318.5+140305 (Abdalla et al. 2018). 3HWC J1922+140 could be a composite of different astrophysical origins. Table 4 shows the constraints on the hadronic fraction, which range from 51% to 85%.

5. SUMMARY AND CONCLUSION

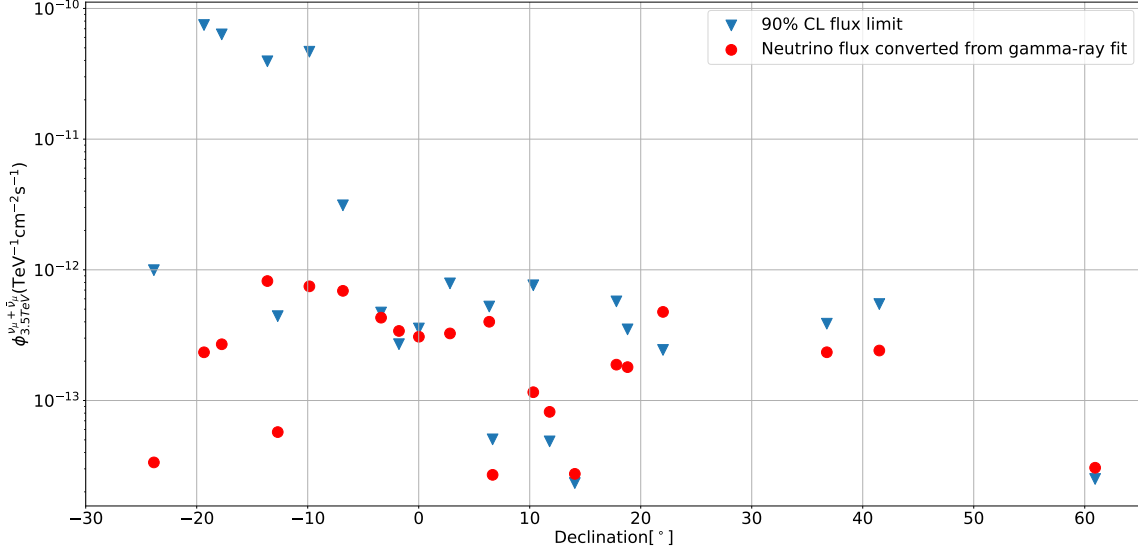


Figure 4. Neutrino 90% CL flux limit from the individual source search. The blue triangles represent the flux limit and the red dots represent the neutrino flux predicted from the gamma-ray best fit assuming all the gamma-ray emission originated from hadronic interaction. Sources that have a predicted neutrino flux higher than the flux limit are the sources for which we can place a hadronic fraction constraint.

Name	α	β	Neutrino 90% CL flux limit [$\text{TeV}^{-1}\text{cm}^{-2}\text{s}^{-1}$]	p-value	Hadronic fraction limit
3HWC J1847-017	-2.66	0.09	2.70×10^{-13}	1	0.79
3HWC J1914+118	-2.69	0	4.87×10^{-14}	1	0.59
3HWC J1922+140	-2.77	0	2.33×10^{-14}	1	0.85
3HWC J0534+220	-2.82	0.12	2.44×10^{-13}	0.36	0.51
3HWC J2227+610	-2.42	0	2.51×10^{-14}	1	0.82

Table 4. Table showing the sources that have a neutrino 90% CL flux limit lower than the predicted neutrino flux at 3.5 TeV when assuming the source is hadronic. The p-value is the pre-trial p-value from the individual source search and a p-value of 1 corresponds to a TS of 0 in the search. The hadronic fraction limit is the ratio between the flux limit and the predicted neutrino flux at 3.5 TeV, representing the maximum hadronic fraction assuming the leptonic emission shares a similar spectral shape.

In this study, we present a new method for performing multi-messenger spectral fits with the 3ML software framework (Vianello et al. 2017) using HAWC and IceCube data. We performed a joint fit using HAWC and IceCube data to search for neutrino emission from potential Galactic PeVatrons. No significant neutrino emission was observed. The most significant source from the joint fit is 3HWC J2019+367 with the lowest pre-trial p-value of 0.07, corresponding to a post-trial p-value of 0.21. A binomial test for an excess distributed over several sources was performed. The binomial test gave a minimum p-value of 0.09, obtained for the six most significant sources. This corresponds to a post-trial p-value of 0.34. After trial correction for the two searches, the overall post-trial p-value is 0.37. We calculated upper limits at 90% confidence level on the neutrino flux, assuming the spectral form corresponding to the best fit for gamma rays. We found that five sources have a neutrino flux limit that is lower than the predicted neutrino flux of a purely hadronic source. We conclude that these five sources cannot be purely hadronic and constrain the hadronic fraction of these sources. Next-generation neutrino detectors can improve our understanding of the physical processes of these TeV gamma-ray emitters. The proposed IceCube-Gen2 detector (Aartsen et al. 2021), with an increased effective area compared to IceCube, is expected to become up to five times more sensitive to galactic neutrino sources. Several neutrino experiments, such as the proposed Pacific Ocean Neutrino Experiment (P-ONE) (Agostini et al. 2020), Tropical Deep-sea Neutrino Telescope (TRIDENT) (Ye et al. 2023), KM3NeT (currently under construction)

(Margiotta 2014) and Baikal-GVD (operating and undergoing upgrade) (Avrerin et al. 2022), are located in the northern hemisphere and have the potential to detect galactic neutrino sources near the galactic center. The proposed SWGO experiment, which is a ground-based gamma-ray water Cherenkov observatory in the southern hemisphere, would be able to discover more TeV gamma rays sources in the southern sky and candidates of Galactic PeVatrons (Huentemeyer et al. 2019).

14 HAWC: We acknowledge the support from: the US National Science Foundation (NSF); the US Department of Energy
 15 Office of High-Energy Physics; the Laboratory Directed Research and Development (LDRD) program of Los Alamos
 16 National Laboratory; Consejo Nacional de Ciencia y Tecnología (CONACyT), México, grants 271051, 232656, 260378,
 17 179588, 254964, 258865, 243290, 132197, A1-S-46288, A1-S-22784, CF-2023-I-645, cátedras 873, 1563, 341, 323, Red
 18 HAWC, México; DGAPA-UNAM grants IG101323, IN111716-3, IN111419, IA102019, IN106521, IN114924, IN110521
 19 , IN102223; VIEP-BUAP; PIFI 2012, 2013, PROFOCIE 2014, 2015; the University of Wisconsin Alumni Research
 20 Foundation; the Institute of Geophysics, Planetary Physics, and Signatures at Los Alamos National Laboratory; Polish
 21 Science Centre grant, DEC-2017/27/B/ST9/02272; Coordinación de la Investigación Científica de la Universidad Mi-
 22 choacana; Royal Society - Newton Advanced Fellowship 180385; Generalitat Valenciana, grant CIDEAGENT/2018/034;
 23 The Program Management Unit for Human Resources & Institutional Development, Research and Innovation, NXPO
 24 (grant number B16F630069); Coordinación General Académica e Innovación (CGAI-UdeG), PRODEP-SEP UDG-CA-
 25 499; Institute of Cosmic Ray Research (ICRR), University of Tokyo. H.F. acknowledges support by NASA under award
 26 number 80GSFC21M0002. We also acknowledge the significant contributions over many years of Stefan Westerhoff,
 27 Gaurang Yodh and Arnulfo Zepeda Domínguez, all deceased members of the HAWC collaboration. Thanks to Scott
 28 Delay, Luciano Díaz and Eduardo Murrieta for technical support.

29 IceCube: The IceCube collaboration acknowledges the significant contributions to this manuscript from Kwok Lung
 30 Fan. The authors gratefully acknowledge the support from the following agencies and institutions: USA – U.S. National
 31 Science Foundation-Office of Polar Programs, U.S. National Science Foundation-Physics Division, U.S. National Science
 32 Foundation-EPSCoR, U.S. National Science Foundation-Office of Advanced Cyberinfrastructure, Wisconsin Alumni
 33 Research Foundation, Center for High Throughput Computing (CHTC) at the University of Wisconsin–Madison,
 34 Open Science Grid (OSG), Partnership to Advance Throughput Computing (PATH), Advanced Cyberinfrastructure
 35 Coordination Ecosystem: Services & Support (ACCESS), Frontera computing project at the Texas Advanced Comput-
 36 ing Center, U.S. Department of Energy-National Energy Research Scientific Computing Center, Particle astrophysics
 37 research computing center at the University of Maryland, Institute for Cyber-Enabled Research at Michigan State
 38 University, Astroparticle physics computational facility at Marquette University, NVIDIA Corporation, and Google
 39 Cloud Platform; Belgium – Funds for Scientific Research (FRS-FNRS and FWO), FWO Odysseus and Big Science
 40 programmes, and Belgian Federal Science Policy Office (Belspo); Germany – Bundesministerium für Bildung und
 41 Forschung (BMBF), Deutsche Forschungsgemeinschaft (DFG), Helmholtz Alliance for Astroparticle Physics (HAP),
 42 Initiative and Networking Fund of the Helmholtz Association, Deutsches Elektronen Synchrotron (DESY), and High
 43 Performance Computing cluster of the RWTH Aachen; Sweden – Swedish Research Council, Swedish Polar Research
 44 Secretariat, Swedish National Infrastructure for Computing (SNIC), and Knut and Alice Wallenberg Foundation; Eu-
 45 ropean Union – EGI Advanced Computing for research; Australia – Australian Research Council; Canada – Natural
 46 Sciences and Engineering Research Council of Canada, Calcul Québec, Compute Ontario, Canada Foundation for
 47 Innovation, WestGrid, and Digital Research Alliance of Canada; Denmark – Villum Fonden, Carlsberg Foundation,
 48 and European Commission; New Zealand – Marsden Fund; Japan – Japan Society for Promotion of Science (JSPS)
 49 and Institute for Global Prominent Research (IGPR) of Chiba University; Korea – National Research Foundation of
 50 Korea (NRF); Switzerland – Swiss National Science Foundation (SNSF).

APPENDIX

A. LIKELIHOOD FORMALISM

HAWC performs a binned likelihood analysis for studying gamma-ray sources. In this analysis, we use the energy binning, the fraction of PMTs hit (f_{hit}) binning, and also Healpix Nside=1024 spatial binning. We calculate the

expected background for each bin by applying direct integration using the zenith distribution of all events passing the gamma/hadron cuts. The technique of direct integration is described in previous HAWC publications (Abeysekara et al. 2019c). The expected excess in every bin is calculated based on the physics model and the detector response of HAWC. The total log-likelihood is the sum of the Poisson log-likelihood of each bin and pixel.

$$\ln \mathcal{L}_{HAWC} = \sum_j^{N_{bin}} \sum_i^{N_{pixels}} \ln \frac{(b_{ij} + e_{ij}f)^{d_{ij}} e^{-(b_{ij} + e_{ij}f)}}{d_{ij}!} \quad (\text{A1})$$

where b_{ij} is the expected background at bin j and pixel i , e_{ij} is the expected excess per unit flux given the model at bin j and pixel i , f is the flux and d_{ij} is the actual count in bin j and pixel i . Index j loops over the energy and $fhit$ bin and index i loops over the number of pixels in the region of interest.

For IceCube, we perform an unbinned likelihood analysis. The total likelihood is given by

$$\mathcal{L}_{IceCube} = \prod_i^N L_i(\vec{\theta}, \vec{D}_i) = \prod_i^N \left(\frac{n_s}{N} S(\vec{\theta}, \vec{D}_i) + \frac{N - n_s}{N} B(\vec{D}_i) \right), \quad (\text{A2})$$

where $\vec{\theta}$ represents the properties of the source hypothesis like location, morphology, and spectrum. L_i is the likelihood of the event i . The parameter vector \vec{D}_i represents the reconstruction information of the event i , including reconstructed energy, direction, and estimated angular error. N is the total number of events and n_s is the number of signal neutrinos. S and B are the signal probability density function (PDF) and background probability density function, each consisting of a product of a spatial likelihood and an energy likelihood. A detailed description of the IceCube likelihood for extended sources can be found in Abbasi et al. (2023a). Since the background likelihood only depends on the reconstructed information of the event and does not depend on the source hypothesis, it is a constant during the fitting process. Therefore, we can divide the likelihood by the likelihood of the background-only hypothesis to get the likelihood ratio which is still a valid likelihood. We rewrite the IceCube log-likelihood to be

$$\ln \mathcal{L}_{IceCube} = \sum_i^N \ln \left(\frac{n_s}{N} \left(\frac{S(\vec{D}_i, \vec{\theta})}{B(\vec{D}_i)} - 1 \right) + 1 \right). \quad (\text{A3})$$

Since HAWC and IceCube measurements are independent, the total log-likelihood for the joint fit is the addition of the HAWC log-likelihood and IceCube log-likelihood.

$$\ln \mathcal{L}_{HAWC} + \ln \mathcal{L}_{IceCube} = \sum_j^{N_{bin}} \sum_i^{N_{pixels}} \ln \frac{(b_{ij} + e_{ij}f)^{d_{ij}} e^{-(b_{ij} + e_{ij}f)}}{d_{ij}!} + \sum_i^N \ln \left(\frac{n_s}{N} \left(\frac{S(\vec{D}_i, \vec{\theta})}{B(\vec{D}_i)} - 1 \right) + 1 \right). \quad (\text{A4})$$

The combined log-likelihood is then maximized over the free parameters in the model.

B. PRE-TRIAL P-VALUES OF THE JOINT SEARCH

Table 5 shows the pre-trial p-value of each source.

C. ICECUBE SYSTEMATICS

In this analysis, we consider the effect of uncertainties on the scattering and absorption of light in the ice, uncertainty in DOM efficiency, and uncertainty in the modeling of ice properties. We consider $\pm 5\%$ uncertainty in absorption and scattering, $\pm 10\%$ in DOM efficiency, and uncertainty in hole ice modeling parameters as described in Eller et al. (2023). The method of handling the systematic uncertainties is similar to the one previously used in IceCube's measurement of the diffuse neutrino flux (Abbasi et al. 2022b). We use different simulation data sets, each with the value of one parameter changed to account for its systematic uncertainty. The change in sensitivity for the joint analysis as compared to the baseline was calculated for the different sources of systematic uncertainties, and these changes were added in quadrature. Table 6 shows the total systematic uncertainty on the neutrino 90% CL flux limit from each source. The final neutrino flux limit of each source is increased by the total systematic uncertainty and is shown in table 3.

Name	pre-trial p-value	post-trial p-value
3HWC J0534+220	0.36	-
3HWC J0634+067	0.19	-
3HWC J1757-240	1	-
3HWC J1809-190	1	-
3HWC J1813-125	1	-
3HWC J1813-174	0.70	-
3HWC J1825-134	1	-
3HWC J1831-095	1	-
3HWC J1837-066	1	-
3HWC J1843-034	1	-
3HWC J1847-017	1	-
3HWC J1849+001	1	-
3HWC J1857+027	0.13	-
3HWC J1908+063	0.10	-
3HWC J1912+103	0.08	-
3HWC J1914+118	1	-
3HWC J1922+140	1	-
3HWC J1928+178	0.14	-
3HWC J1930+188	1	-
3HWC J2019+367	0.07	0.21
3HWC J2031+415	0.08	-
3HWC J2227+610	1	-

Table 5. The pre-trial p-value and the post-trial p-value of the joint fit. A p-value of 1 corresponds to a TS equal to 0.

Name	Total systematic uncertainties
3HWC J0534+220	18%
3HWC J0634+067	25%
3HWC J1757-240	25%
3HWC J1809-190	39%
3HWC J1813-125	27%
3HWC J1813-174	54%
3HWC J1825-134	30%
3HWC J1831-095	40%
3HWC J1837-066	33%
3HWC J1843-034	19%
3HWC J1847-017	21%
3HWC J1849+001	19%
3HWC J1857+027	18%
3HWC J1908+063	18%
3HWC J1912+103	21%
3HWC J1914+118	20%
3HWC J1922+140	14%
3HWC J1928+178	13%
3HWC J1930+188	23%
3HWC J2019+367	14%
3HWC J2031+415	16%
3HWC J2227+610	30%

Table 6. The total IceCube systematics for each source. We add 1 to the numbers and then multiply by the neutrino 90% CL flux limit computed from baseline Monte Carlo to obtain the final neutrino flux limit.

REFERENCES

- Aartsen, M. G., Abbasi, R., Ackermann, M., et al. 2014, *Journal of Instrumentation*, 9, P03009, doi: [10.1088/1748-0221/9/03/P03009](https://doi.org/10.1088/1748-0221/9/03/P03009)
- Aartsen, M. G., Ackermann, M., Adams, J., et al. 2014, *ApJ*, 796, 109, doi: [10.1088/0004-637X/796/2/109](https://doi.org/10.1088/0004-637X/796/2/109)
- . 2017, *Journal of Instrumentation*, 12, P03012, doi: [10.1088/1748-0221/12/03/P03012](https://doi.org/10.1088/1748-0221/12/03/P03012)
- . 2020a, *PhRvL*, 124, 051103, doi: [10.1103/PhysRevLett.124.051103](https://doi.org/10.1103/PhysRevLett.124.051103)
- . 2020b, *PhRvL*, 124, 051103, doi: [10.1103/PhysRevLett.124.051103](https://doi.org/10.1103/PhysRevLett.124.051103)
- Aartsen, M. G., Abbasi, R., Ackermann, M., et al. 2021, *Journal of Physics G Nuclear Physics*, 48, 060501, doi: [10.1088/1361-6471/abbd48](https://doi.org/10.1088/1361-6471/abbd48)
- Abbasi, R., Ackermann, M., Adams, J., et al. 2009, *NIM A*, 601, 294, doi: [10.1016/j.nima.2009.01.001](https://doi.org/10.1016/j.nima.2009.01.001)
- Abbasi, R., Abdou, Y., Abu-Zayyad, T., et al. 2010, *NIM A*, 618, 139, doi: <https://doi.org/10.1016/j.nima.2010.03.102>
- Abbasi, R., Ackermann, M., Adams, J., et al. 2021, in *Proceedings of 37th International Cosmic Ray Conference — PoS(ICRC2021)*, Vol. 395, 1098, doi: [10.22323/1.395.1098](https://doi.org/10.22323/1.395.1098)
- Abbasi, R., Ackermann, M., Adams, J., et al. 2022a, *The Astrophysical Journal*, 939, 116, doi: [10.3847/1538-4357/ac9785](https://doi.org/10.3847/1538-4357/ac9785)
- . 2022b, *The Astrophysical Journal*, 928, 50, doi: [10.3847/1538-4357/ac4d29](https://doi.org/10.3847/1538-4357/ac4d29)
- . 2023a, *The Astrophysical Journal Letters*, 945, L8, doi: [10.3847/2041-8213/acb933](https://doi.org/10.3847/2041-8213/acb933)
- . 2023b, *Science*, 380, 1338, doi: [10.1126/science.adc9818](https://doi.org/10.1126/science.adc9818)
- . 2023c, *The Astrophysical Journal*, 956, 20, doi: [10.3847/1538-4357/acf713](https://doi.org/10.3847/1538-4357/acf713)
- Abbasi, R. U., Abe, M., Abu-Zayyad, T., et al. 2018, *ApJ*, 865, 74, doi: [10.3847/1538-4357/aada05](https://doi.org/10.3847/1538-4357/aada05)
- Abdalla, H., Abramowski, A., Aharonian, F., et al. 2018, *A&A*, 612, A1, doi: [10.1051/0004-6361/201732098](https://doi.org/10.1051/0004-6361/201732098)
- Abeysekara, A., Albert, A., Alfaro, R., et al. 2023, *Nuclear Instruments and Methods in Physics Research Section A: Accelerators, Spectrometers, Detectors and Associated Equipment*, 1052, 168253, doi: <https://doi.org/10.1016/j.nima.2023.168253>
- Abeysekara, A. U., Albert, A., Alfaro, R., et al. 2019a, *The Astrophysical Journal*, 881, 134, doi: [10.3847/1538-4357/ab2f7d](https://doi.org/10.3847/1538-4357/ab2f7d)
- . 2019b, *The Astrophysical Journal*, 881, 134, doi: [10.3847/1538-4357/ab2f7d](https://doi.org/10.3847/1538-4357/ab2f7d)
- . 2019c, *The Astrophysical Journal*, 881, 134, doi: [10.3847/1538-4357/ab2f7d](https://doi.org/10.3847/1538-4357/ab2f7d)
- Abeysekara, A. U., Albert, A., Alfaro, R. J., et al. 2021, in *Proceedings of 37th International Cosmic Ray Conference — PoS(ICRC2021)*, Vol. 395, 828, doi: [10.22323/1.395.0828](https://doi.org/10.22323/1.395.0828)
- Abramowski, A., Aharonian, F., Benkhali, F. A., et al. 2016, *Nature*, 531, 476, doi: [10.1038/nature17147](https://doi.org/10.1038/nature17147)
- Agostini, M., Böhmer, M., Bosma, J., et al. 2020, *Nature Astronomy*, 4, 913, doi: [10.1038/s41550-020-1182-4](https://doi.org/10.1038/s41550-020-1182-4)
- Ahlers, M., & Murase, K. 2014, *PhRvD*, 90, 023010, doi: [10.1103/PhysRevD.90.023010](https://doi.org/10.1103/PhysRevD.90.023010)
- Albert, A., Alfaro, R., Alvarez, C., et al. 2020a, *The Astrophysical Journal Letters*, 896, L29, doi: [10.3847/2041-8213/ab96cc](https://doi.org/10.3847/2041-8213/ab96cc)
- . 2020b, *The Astrophysical Journal*, 905, 76, doi: [10.3847/1538-4357/abc2d8](https://doi.org/10.3847/1538-4357/abc2d8)
- Albert, A., Alfaro, R., Alvarez, C., et al. 2021, *ApJL*, 907, L30, doi: [10.3847/2041-8213/abd77b](https://doi.org/10.3847/2041-8213/abd77b)
- . 2022, *ApJ*, 928, 116, doi: [10.3847/1538-4357/ac56e5](https://doi.org/10.3847/1538-4357/ac56e5)
- Avrorin, A. V., Avrorin, A. D., Ayinutdinov, V. M., et al. 2022, *Soviet Journal of Experimental and Theoretical Physics*, 134, 399, doi: [10.1134/S1063776122040148](https://doi.org/10.1134/S1063776122040148)
- Bell, A. R., Schure, K. M., Reville, B., & Giacinti, G. 2013, *Monthly Notices of the Royal Astronomical Society*, 431, 415, doi: [10.1093/mnras/stt179](https://doi.org/10.1093/mnras/stt179)
- Blandford, R. D., & Ostriker, J. P. 1978, *ApJL*, 221, L29, doi: [10.1086/182658](https://doi.org/10.1086/182658)
- Bykov, A. M., Marcowith, A., Amato, E., et al. 2020, *SSRv*, 216, 42, doi: [10.1007/s11214-020-00663-0](https://doi.org/10.1007/s11214-020-00663-0)
- Cao, Z., Aharonian, F. A., An, Q., et al. 2021, *Nature*, 594, 33, doi: [10.1038/s41586-021-03498-z](https://doi.org/10.1038/s41586-021-03498-z)
- Di Palma, I., Guetta, D., & Amato, E. 2017, *ApJ*, 836, 159, doi: [10.3847/1538-4357/836/2/159](https://doi.org/10.3847/1538-4357/836/2/159)
- Eller, P., Rongen, M., Abbasi, R., et al. 2023, in *Proceedings of 38th International Cosmic Ray Conference — PoS(ICRC2023)*, Vol. 444, 1034, doi: [10.22323/1.444.1034](https://doi.org/10.22323/1.444.1034)
- Gabici, S., & Aharonian, F. A. 2007, *ApJL*, 665, L131, doi: [10.1086/521047](https://doi.org/10.1086/521047)
- Hess, V. F. 1912, *Phys. Z.*, 13, 1084
- Hinton, J. A., & Hofmann, W. 2009, *ARA&A*, 47, 523, doi: [10.1146/annurev-astro-082708-101816](https://doi.org/10.1146/annurev-astro-082708-101816)
- Huentemeyer, P., BenZvi, S., Dingus, B., et al. 2019, in *Bulletin of the American Astronomical Society*, Vol. 51, 109, doi: [10.48550/arXiv.1907.07737](https://doi.org/10.48550/arXiv.1907.07737)
- Klein, O., & Nishina, T. 1929, *Zeitschrift fur Physik*, 52, 853, doi: [10.1007/BF01366453](https://doi.org/10.1007/BF01366453)

- Margiotta, A. 2014, *Nuclear Instruments and Methods in Physics Research Section A: Accelerators, Spectrometers, Detectors and Associated Equipment*, 766, 83, doi: <https://doi.org/10.1016/j.nima.2014.05.090>
- Vianello, G., Lauer, R. J., Burgess, J. M., et al. 2017, in *Proceedings of 7th International Fermi Symposium — PoS(IFS2017)*, Vol. 312, 130, doi: [10.22323/1.312.0130](https://doi.org/10.22323/1.312.0130)
- Wakely, S. P., & Horan, D. 2008, in *International Cosmic Ray Conference*, Vol. 3, *International Cosmic Ray Conference*, 1341–1344
- Wilks, S. S. 1938, *The Annals of Mathematical Statistics*, 9, 60. <http://www.jstor.org/stable/2957648>
- Ye, Z. P., Hu, F., Tian, W., et al. 2023, *Nature Astronomy*, 7, 1497, doi: [10.1038/s41550-023-02087-6](https://doi.org/10.1038/s41550-023-02087-6)
- Yun-Carcamo, S. L., Albert, A., Alfaro, R. J., et al. 2023, in *Proceedings of 38th International Cosmic Ray Conference — PoS(ICRC2023)*, Vol. 444, 697, doi: [10.22323/1.444.0697](https://doi.org/10.22323/1.444.0697)